Quantification of Secondary Electron Doping Contrast in the Scanning Electron Microscope on 4H-SiC

Moser Maximilian[1,a*], Pobegen Gregor[,1,b], and Smoliner Jürgen[2,c]

[1]KAI GmbH, Europastraße 8, Villach, Austria

[2]Institute for Solid State Electronics, TU Vienna, Gußhausstraße 25-25a, Vienna, Austria

[a]maximilian.moser@k-ai.at, [b]gregor.pobegen@k-ai.at, [c]juergen.smoliner@tuwien.ac.at

Abstract. We discuss the quantification of the secondary electron doping contrast in the scanning electron microscope on 4H-SiC. It has been observed and studied at length mostly on silicon, but no conclusive theoretical model has been proposed yet. Therefore, we propose a simple physical model that allows for a quantification of the doping contrast. It is based on the changes in effective ionization energy for different doping concentrations and types. For a better agreement between our model and the experiment, a locally increased temperature of the electron system or separate quasi Fermi levels for electrons and holes have to be assumed. A line profile of the sample under investigation is compared with a SRIM simulation of the corresponding implant and shows very good agreement.

Introduction

To enable the development of future improved SiC power devices, the knowledge of the effective doping concentration and electric field distribution is crucial. Due to the sub-micrometer scales of interest, a very good spatial resolution is required. Our method of choice is the secondary electron (SE) doping contrast in the scanning electron microscope (SEM) which shows clear advantages compared to atomic force microscopy (AFM) based approaches, such as scanning capacitance microscopy (SCM) and scanning spreading resistance microscopy (SSRM), such as the increased spatial resolution, simpler sample preparation and scalability for production use.

The SE doping contrast is usually understood as the effect, where acceptor doped regions appear brighter than donor doped areas in the SEM. It has already been described by other authors in many publications including, but not limited to [1–13]. Most of these publications have focused on silicon and described the doping contrast qualitatively. Ref. [5] has investigated the doping contrast on 4H-SiC and [10] has attempted a quantification using a Monte-Carlo simulation and achieved a qualitatively good agreement with the experiment. The most prevalent mechanisms proposed for the SE doping contrast are surface band bending [8], differences in work function [9] and stray electric fields at the sample surface [5]. Many of the previous papers have focused on maximizing the SE doping contrast in an effort to identify and better understand the mechanisms contributing to it. Here, we develop a method that allows for the 8 or 16 bit gray values of SEM images to be converted to a doping concentration via a simple physical model.

Model and Conversion

Our approach relies on the differences in effective ionization energy. The model is based on the assumption that the primary electron beam generates electron-hole pairs in the sample. The generated electron-hole pairs fill the surface states and suppress the surface band bending. This leads to flat-band condition, which is similar to the flat-band condition caused by ultraviolet light radiation [14]. The model is similar to the one discussed in [2], but with key differences being the aforementioned flat-band condition, the addition of a higher local temperature of the electron system and quasi Fermi level splitting. In addition, a small positive sample bias is introduced to shift the SE spectrum for monotonic contrast.
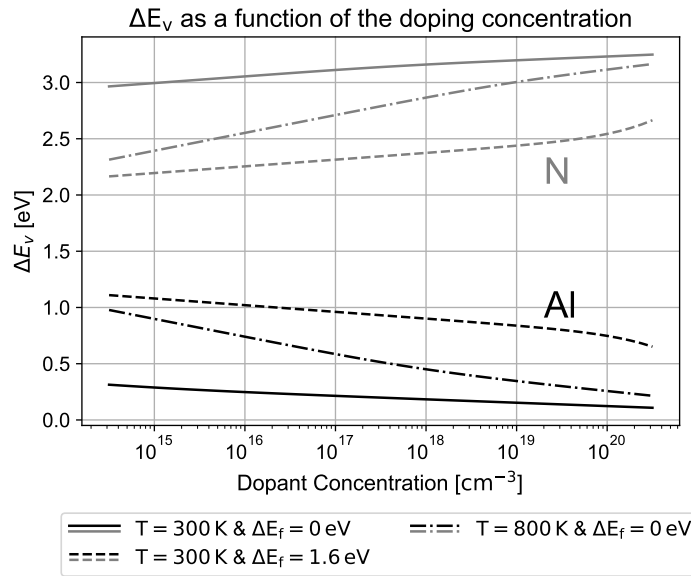
Fig. 1: The physical model that forms the basis for the conversion of gray values to the doping concentrations. For SEs to be detected, they need to have enough energy to surpass the detection energy level E_{detect}.

The primary origin of the SEs, that reach the detector of the microscope, is the valence band. This can be safely assumed, as even at very high n-doping concentrations of 10^{20} cm^{-3} the number of electrons in the conduction band is magnitudes smaller than the concentration of atoms ($\sim 5 \times 10^{22}$ cm^{-3}) with multiple valence electrons each.

The SEs that are ionized from the sample still need to pass the detection energy barrier E_{detect} to get detected. This position of E_{detect} above the vacuum level E_{vac} can be varied by adding a positive bias to the sample stage in the SEM. Our model is summarized in Fig. 1. The electrons originating from the valence band need to have enough energy to not only get ejected from the sample by passing E_{vac}, but also pass E_{detect}. A smaller $\Delta E_{effective}$ will result in a larger number of SEs that can be detected. Because its exact value is not known precisely, we need to express the $\Delta E_{effective}$ differences between n- and p-doped areas through a known quantity to quantify the doping contrast:

$$\Delta E_{effective} = E_{detect} - E_v = \underbrace{E_{detect} - E_f}_{=const.} + \underbrace{E_f - E_v}_{=\Delta E_v} = const. + \Delta E_v \qquad (1)$$

The potential difference between E_{detect} and the Fermi level E_f is constant across the whole sample. Therefore, we subtract it, reducing $\Delta E_{effective}$ to ΔE_v, which is defined as the energetic difference between E_f and ΔE_v:

$$\Delta E_v = E_f - E_v \qquad (2)$$

To convert the gray values of the SEM image, we need to calculate ΔE_v, which can be calculated from E_f using Eq. (2). E_f is calculated by solving the charge neutrality equation

$$n(E_f, T) + N_A^*(E_f, T, N_{Al}) = p(E_f, T) + N_D^*(E_f, T, N_N) \qquad (3)$$

numerically via bisection for E_f for a given doping concentration. In this equation $n(E_f, T)$ is the concentration of electrons, $p(E_f, T)$ the concentration of holes, $N_A^*(E_f, T, N_{Al})$ the concentration of ionized acceptors and $N_D^*(E_f, T, N_N)$ the number of ionized donors. ΔE_v as a function of the temperature and the doping concentration for n- and p-doping is shown in Fig. 2.

Fig. 2: ΔE_v as a function of the doping concentration for n- and p-doped (N & Al) SiC. The solid lines represent the calculation at room temperature without quasi Fermi level splitting, the dashed lines represent the calculation at 800 K without quasi Fermi level splitting and the dash-dotted lines represent the calculation at room temperature with a quasi Fermi level splitting of 1.6 eV. Gray represents n-doping and black represents p-doping.

To convert the gray values to doping concentrations, two regions in the SEM image, where the doping concentration is known, have to be marked by the user. Their gray values are then linked to their corresponding ΔE_v. Now each gray value can be linearly inter- or extrapolated to obtain the corresponding ΔE_v. By inverting the relation in Fig. 2 the doping concentration can be obtained. These two steps can be summarized in a conversion function as shown in Fig. 3.

Due to the generation of electron-hole pairs by the primary electrons of the electron beam, the conversion assuming room temperature grossly over- and underestimates the aluminum doping concentration for input gray values above and below the reference, respectively. Therefore we introduce two approaches to take the additional electron-hole pairs and their effects on the calculation of E_f into account. In the first approach, we assume a higher local temperature of the electron system. For the measurement presented later in this paper and many others a temperature of 800 K fits the reference well. Alternatively, the generation of electron-hole pairs can be viewed as local quasi Fermi level splitting ΔE_f, similar to the effect found in photonic devices [15]. The quasi Fermi level splitting is defined symmetrically. The levels for electrons and holes are shifted by $\Delta E_\mathrm{f}/2$ from the reference Fermi level. For the same measurement, the best agreeing ΔE_f was found to be 1.6 eV. This is consistent across different SiC samples when using the same primary electron beam current and calibrations can be easily reused from previous measurements. Increasing the beam current results in a larger quasi Fermi level splitting and a higher temperature needed for this fit. Introducing quasi Fermi level splitting leads to a modification of Eq. (3):

$$n(E_\mathrm{f} + {}^{\Delta E_\mathrm{f}}/_2, T) + N_\mathrm{A}^*(E_\mathrm{f} + {}^{\Delta E_\mathrm{f}}/_2, T, N_\mathrm{Al}) = p(E_\mathrm{f} - {}^{\Delta E_\mathrm{f}}/_2, T) + N_D^*(E_\mathrm{f} - {}^{\Delta E_\mathrm{f}}/_2, T, N_\mathrm{N}) \qquad (4)$$

ΔE_v can be recalculated with these corrections and is shown in Fig. 2. This results in the conversion functions of Fig. 3.

These two functions have a similar gradient around the Al reference doping concentration of 10^{19} cm^{-3}. The discrepancies can be explained by the fundamental differences between the two mod-

els describing the additional electron-hole pairs. The incompatibility and limited validity of some phenomenological models involved in the calculation of the functions may also contribute.

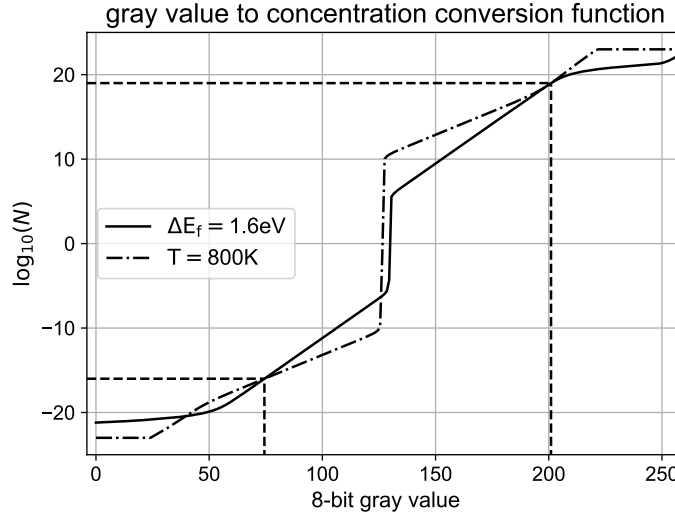### gray value to concentration conversion function

Fig. 3: The 8-bit gray value to doping concentration conversion function for quasi Fermi level splitting (solid) and a higher temperature (dash-dot). The positive values of the y-axis correspond to the $\log_{10}$ of the p-doping (Al) concentration and the negative values correspond to the n-doping (N) concentration. The dashed lines correspond to the two gray value and concentration pairs that were marked by the user. The vertical section at a gray value of 125 is caused by ΔE_v being identical for very low n- and p-doping concentrations.

Materials and Methods

For the acquisition of the below shown images a Hitachi SU8230 SEM was used. The sample was cleaved in air and attached to the sample holder with silver glue. The silver glue was dried in a nitrogen flooded oven at 60°C. For an exact description of the sample see [16]. An acceleration voltage of 1 kV with an extraction current of 5 μA was used. A positive stage bias of 2.5 V was applied to the sample with an external voltage supply. This is necessary to suppress artifacts at the p-n junction in the SEM image. In order to minimize the effects of carbon depositions on the sample surface, each area for imaging was only scanned once when taking the image.

Results and Discussion

In Fig. 4 the algorithm for the conversion from gray values to doping concentration is applied to a line profile of the sample as shown in Fig. 5 (a). It is compared with a SRIM simulation (Stopping Range of Ions in Matter) [17] and both the approaches with a higher temperature and quasi Fermi level splitting fit the implant with a peak at 0.7 μm well. At around 0.1 μm the 10^{20} cm^{-3} concentration peak plateau better agrees with quasi Fermi level splitting. The differences between the concentration profiles of the SEM image and the SRIM concentration profile can be explained by inaccuracies of the SRIM simulation when compared to the ion implantation and subsequent annealing. The deviation at 1 μm is explained by the beginning of the p-n junction, where ΔE_v is mainly influenced by the space charge region. In Fig. 5 (b) the same algorithm is applied to the SEM image of Fig. 5 (a). The values between concentrations of 10^{15} cm^{-3} aluminum and 10^{15} cm^{-3} nitrogen are plotted white for a better visibility of doping concentrations in the relevant scales.

For both Figs. 4 and 5, the aluminum concentration values below 10^{17} cm^{-3} near the space charge region of the p-n junction must be interpreted carefully, as they are likely to be already influenced by the junction.
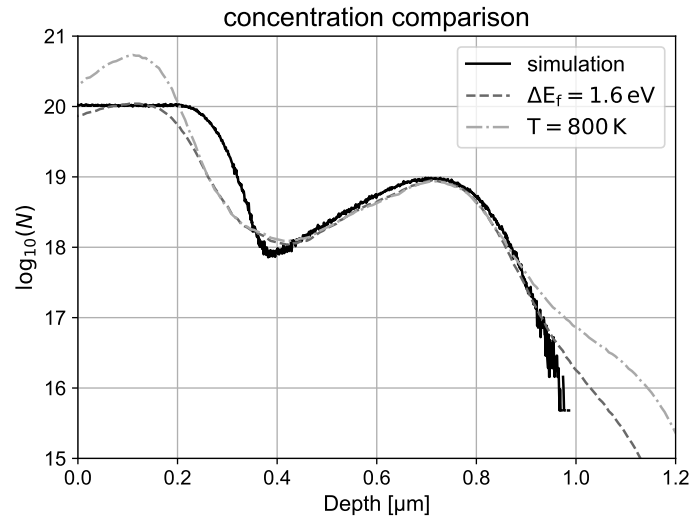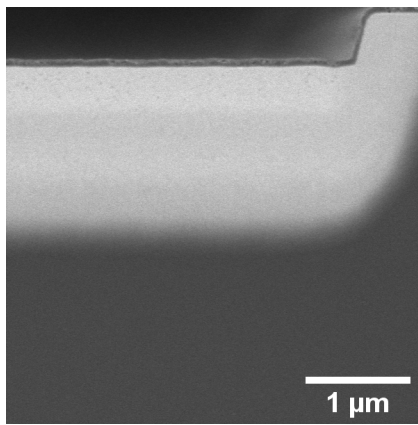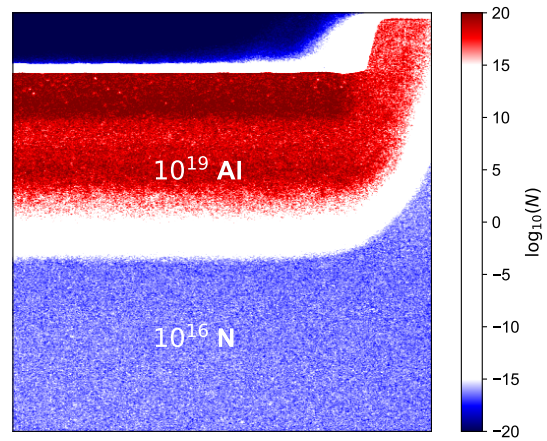

Fig. 4: The vertical line profile of the SEM image in Fig. 5 (a). The conversion used the functions for a temperature of 800 K and for a ΔE_f of 1.6 eV of Fig. 3 and was averaged over a width of 400 pixels. The profiles are compared to the doping concentration profile given by a SRIM simulation.

(a)

(b)

Fig. 5: (a) shows a section of a SEM image of a sample from [16] and (b) shows the same section converted to a doping concentration map with a quasi Fermi level splitting of 1.6 eV. The reference points for the conversion are also indicated and correspond to the dashed lines of Fig. 3. The positive values of the colorbar correspond to the $\log_{10}$ of the p-doping (Al) concentration and the negative values correspond to the n-doping (N) concentration.

Conclusion

We developed a simple physical model to convert the gray values of a SEM image to doping concentrations. The SEM image taken with a positive sample bias of 2.5 V was converted to a map of the doping concentration and the vertical line profile is in good agreement with a SRIM simulation.

Two approaches to account for the imbalance caused by extra electron hole pairs induced by the primary electron beam were developed. The model using quasi Fermi level splitting is in slightly better agreement with the data than the model assuming a higher temperature of the electron system.

Exploiting a variation of the imaging parameters and with a better understanding of the physical processes involved, a quantification of the secondary electron doping contrast without prior knowledge of the sample will be possible.

Acknowledgments

References

[1] D. Perovic, M. Castell, A. Howie, C. Lavoie, T. Tiedje, and J. Cole, "Field-emission SEM imaging of compositional and doping layer semiconductor superlattices," *Ultramicroscopy*, vol. 58, no. 1, pp. 104–113, 1995.

[2] C. P. Sealy, M. R. Castell, and P. R. Wilshaw, "Mechanism for secondary electron dopant contrast in the SEM," *Journal of Electron Microscopy*, vol. 49, no. 2, pp. 311–321, 2000.

[3] S. L. Elliott, R. F. Broom, and C. J. Humphreys, "Dopant profiling with the scanning electron microscope—A study of Si," *Journal of Applied Physics*, vol. 91, no. 11, pp. 9116–9122, 2002.

[4] P. Kazemian, C. Rodenburg, and C. Humphreys, "Effect of experimental parameters on doping contrast of Si p–n junctions in a FEG-SEM," *Microelectronic Engineering*, vol. 73-74, pp. 948–953, 2004.

[5] M. Buzzo, M. Ciappa, and W. Fichtner, "Imaging and dopant profiling of silicon carbide devices by secondary electron dopant contrast," *IEEE Transactions on Device and Materials Reliability*, vol. 6, no. 2, pp. 203–212, 2006.

[6] P. Kazemian, S. A. M. Mentink, C. Rodenburg, and C. J. Humphreys, "High resolution quantitative two-dimensional dopant mapping using energy-filtered secondary electron imaging," *Journal of Applied Physics*, vol. 100, no. 5, p. 054901, 2006.

[7] D. Cooper, R. Truche, P. Rivallin, J.-M. Hartmann, F. Laugier, F. Bertin, A. Chabli, and J.-L. Rouviere, "Medium resolution off-axis electron holography with millivolt sensitivity," *Applied Physics Letters*, vol. 91, no. 14, p. 143501, 2007.

[8] M. Dapor, B. J. Inkson, C. Rodenburg, and J. M. Rodenburg, "A comprehensive Monte Carlo calculation of dopant contrast in secondary-electron imaging," *EPL (Europhysics Letters)*, vol. 82, no. 3, p. 30006, 2008.

[9] I. Volotsenko, M. Molotskii, Z. Barkay, J. Marczewski, P. Grabiec, B. Jaroszewicz, G. Meshulam, E. Grunbaum, and Y. Rosenwaks, "Secondary electron doping contrast: Theory based on scanning electron microscope and Kelvin probe force microscopy measurements," *Journal of Applied Physics*, vol. 107, no. 1, p. 014510, 2010.

[10] A. K. W. Chee, R. F. Broom, C. J. Humphreys, and E. G. T. Bosch, "A quantitative model for doping contrast in the scanning electron microscope using calculated potential distributions and Monte Carlo simulations," *Journal of Applied Physics*, vol. 109, no. 1, p. 013109, 2011.

[11] A. K. W. Chee, "Quantitative Dopant Profiling by Energy Filtering in the Scanning Electron Microscope," *IEEE Transactions on Device and Materials Reliability*, vol. 16, no. 2, pp. 138–148, 2016.

[12] Y. Aizawa, T. Sato, T. Sunaoshi, H. Matsumoto, T. Agemura, S. Torikawa, I. Nakatani, and M. Kiyohara, "High Contrast SEM Observation of Semiconductor Dopant Profile using Triple-Beam® System," *Microscopy and Microanalysis*, vol. 23, no. S1, p. 1508–1509, 2017.

[13] W. Han, A. Srinivasan, A. Banerjee, M. Chew, and A. Khursheed, "Beyond conventional secondary electron imaging using spectromicroscopy and its applications in dopant profiling," *Materials Today Advances*, vol. 2, p. 100012, 2019.

[14] Z. Zhang and J. T. Yates, "Band Bending in Semiconductors: Chemical and Physical Consequences at Surfaces and Interfaces," *Chemical Reviews*, vol. 112, no. 10, pp. 5520–5551, 2012.

[15] M. L. M. Larry A. Coldren, Scott W. Corzine, *Gain and Current Relations*, ch. Four, pp. 157–246. John Wiley & Sons, Ltd, 2012.

[16] K. L. Mletschnig, M. Rommel, G. Pobegen, W. Schustereder, and P. Pichler, "Aluminum Activation in 4H-SiC Measured on Laterally Contacted MOS Capacitors with a Buried Current-Spreading Layer," *Materials Science Forum*, vol. 1062, pp. 38–43, 2022.

[17] J. F. Ziegler, M. Ziegler, and J. Biersack, "SRIM – The stopping and range of ions in matter (2010)," *Nuclear Instruments and Methods in Physics Research Section B: Beam Interactions with Materials and Atoms*, vol. 268, no. 11, pp. 1818–1823, 2010.